

2. A neutron primer: Elastic scattering and the properties of the neutron

Thomas Brückel, IFF, Forschungszentrum Jülich

2.1 Introduction

After we have learnt how neutrons are produced in neutron sources, we will explain in this chapter, how neutrons can be used to study the atomic structure and dynamics of condensed matter systems. We will give a basic introduction into scattering methods in general and then introduce the special properties of neutrons, which make them an invaluable probe for condensed matter research. Neutrons tell us, where the atoms are, how the atoms move and what their atomic magnetic moments do.

Our present understanding of the properties and phenomena of condensed matter science is based on atomic theories. The first question we pose when studying any condensed matter system is the question concerning the internal structure: what are the relevant building blocks (atoms, molecules, colloidal particles, ...) and how are they arranged? The second question concerns the microscopic dynamics: how do these building blocks move and what are their internal degrees of freedom? For magnetic systems, in addition we need to know the arrangement of the microscopic magnetic moments due to spin and orbital angular momentum and their excitation spectra. In principle, the macroscopic response and transport properties, such as specific heat, thermal conductivity, elasticity, viscosity, susceptibility, magnetization etc., which are the quantities of interest for applications, result from the microscopic structure and dynamics. To determine these macroscopic properties from the microscopic information provided by scattering experiments represents a huge challenge to condensed matter theory as we are dealing with an extreme many body problem with typically 10^{23} particles involved. It is a true masterly achievement of mankind that for many solid state systems, such microscopic theories could be developed, based on quantum mechanics and statistical physics.

For the progress of modern condensed matter research, the availability of probes to study structure and dynamics on a microscopic level is therefore essential. Modern scattering techniques can provide all the required information. Radiation, which has a rather weak interaction with the sample under investigation, provides a non-invasive, non-destructive probe for the microscopic structure and dynamics. This has been shown for the first time by W. Friedrich, P. Knipping and M. von Laue in 1912, when interference of x-ray radiation scattered from a single crystal was observed. Max von Laue received the Nobel Prize for the interpretation of these observations. One cannot overestimate this discovery: it was the first definite proof that atoms as the elementary building blocks of condensed matter are arranged in a periodic manner within a crystal. The overwhelming part of our present-day knowledge of the atomic structure of condensed matter is based on x-ray structure investigations. The method has developed rapidly since 1912. With the advent of modern synchrotron x-ray sources, the source brilliance has since then increased by 18 orders of magnitude. Currently X-ray Free Electron Lasers, e. g. the XFEL project (<http://xfel.desy.de/>), are being realized which will increase this brilliance by another 10 orders of magnitude. Nowadays the structure of highly complex biological macromolecules, like the crystal structure of the ribosome, can be determined with atomic resolution. Extremely weak phenomena such as magnetic x-ray scattering can be exploited successfully at modern synchrotron radiation sources. In soft condensed matter research, where one is interested in the dynamics on larger lengths scales, such

as of colloidal particles in solution, light scattering is an important tool besides x-ray scattering. Finally, intense neutron beams have properties, which make them an excellent probe for condensed matter investigations. Neutron scattering is a unique tool to solve magnetic structures and determine magnetic excitations and fluctuations. In soft matter and life science, neutrons excel due to the possibility to apply contrast variation techniques by selective deuteration of molecules or molecular subunits. Neutrons give access to practically all lengths scales relevant in condensed matter investigations from the sub-atomic level of some pm up to about 1000 nm. They are particularly well suited for investigations of the movement of atoms and molecules. Similar to x-rays, the experimental techniques are in rapid evolution, mainly due to the advent of new neutron optical devices, but also of new sources. The new spallation sources, such as the American Spallation Neutron Source SNS (<http://www.sns.gov/>) or the proposed European Spallation Source ESS (http://neutron.neutron-eu.net/n_ess) will increase the capabilities of neutron investigations in condensed matter science drastically in the years to come.

This lecture is organized as follows: First we give a very basic introduction into elementary scattering theory for elastic scattering, which is valid for any probe. Then a more rigorous derivation in the framework of the Born series follows. This section can be skipped by beginners, but is provided for completeness.

We will introduce the concepts of coherence and pair correlation functions. Then we will discuss, which probes are most relevant for condensed matter investigations and present in some detail the interaction of neutrons with matter leading to the absorption and scattering cross-sections. More details can be found in [1 - 5].

We will frequently make use of the particle-wave dualism of quantum mechanics, which tells us that the radiation used in the scattering process can be described in a wave picture, whenever we are interested in interference phenomena, and in a particle picture, when the interaction with matter is relevant, e. g. for the detection process.

2.2 Elementary scattering theory: Elastic scattering

Throughout this lecture we assume that the atoms within our sample are rigidly fixed on equilibrium positions in space. Therefore we only look at those processes, in which the recoil is being transferred to the sample as a whole so that the energy change for the radiation is negligible and the scattering process appears to be elastic. In subsequent lectures, this restriction will be dropped and so-called inelastic scattering processes will be discussed. These are due to excitations or internal fluctuations in the sample, which give rise to an energy change of the radiation during the scattering process.

A sketch of the scattering experiment is shown in Figure 2.1.

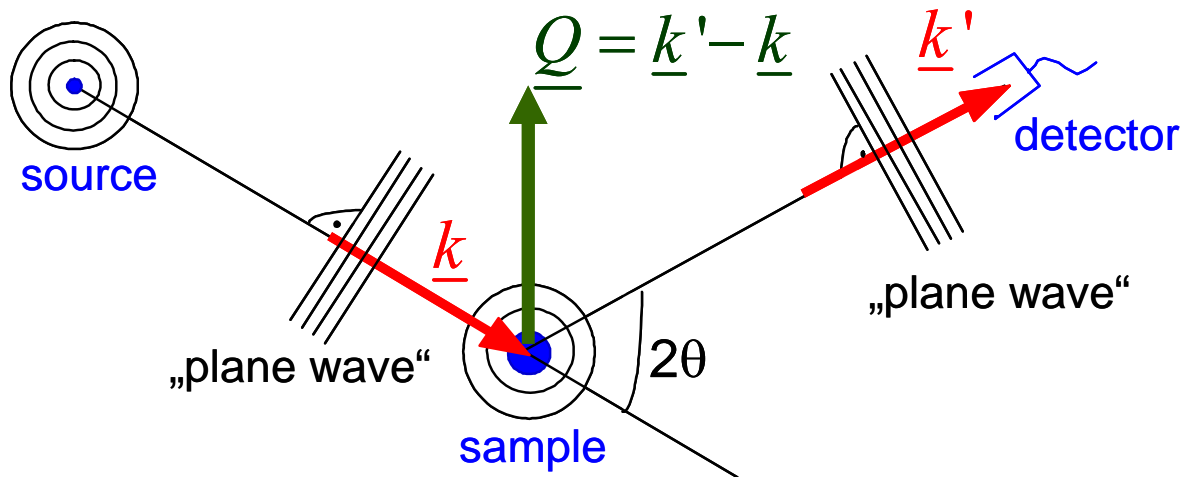


Fig. 2.1: A sketch of the scattering process in the Fraunhofer approximation in which it is assumed that plane waves are incident on sample and detector due to the fact that the distances source-sample and sample-detector, respectively, are significantly larger than the size of the sample.

Here we assume the so-called *Fraunhofer approximation*, where the size of the sample is much smaller than the distance between sample and source and the distance between sample and detector, respectively. This assumption holds in all cases discussed in this lecture. In addition we assume that the source emits radiation of one given energy, i. e. so-called *monochromatic* radiation. Then the wave field incident on the sample can be considered as a plane wave, which is completely described by a wave vector \underline{k} . The same holds for the wave incident on the detector, which can be described by a vector \underline{k}' . In the case of elastic scattering (diffraction) we have

$$k = |\underline{k}| = |\underline{k}'| = k' = \frac{2\pi}{\lambda} \quad (2.1)$$

Let us define the so-called *scattering vector* by

$$\underline{Q} = \underline{k}' - \underline{k} \quad (2.2)$$

$\hbar\underline{Q}$ represents the momentum transfer during scattering, since according to de Broglie, the momentum of the particle corresponding to the wave with wave vector \underline{k} is given by $\underline{p} = \hbar\underline{k}$. The magnitude of the scattering vector can be calculated from wavelength λ and scattering angle 2θ as follows

$$Q = |\underline{Q}| = \sqrt{k^2 + k'^2 - 2kk' \cos 2\theta} \Rightarrow Q = \frac{4\pi}{\lambda} \sin \theta \quad (2.3)$$

A scattering experiment comprises the measurement of the intensity distribution as a function of the scattering vector $I(Q)$. The scattered intensity is proportional to the so-called *cross section*, where the proportionality factors arise from the detailed geometry of the experiment. For a definition of the scattering cross section, we refer to Figure 2.2.

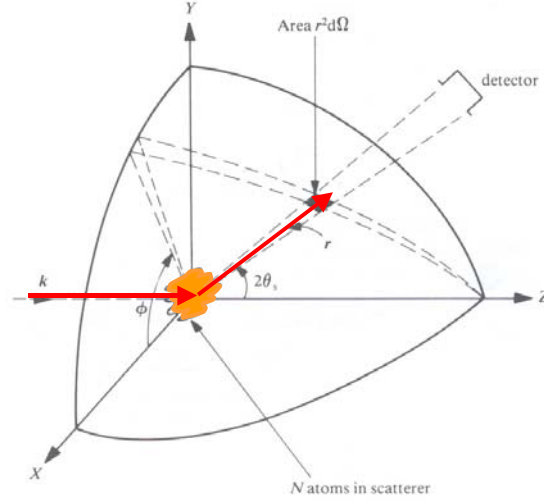


Fig. 2.2: Geometry used for the definition of the scattering cross section.

If n' particles are scattered per second into the solid angle $d\Omega$ seen by the detector under the scattering angle 2θ and into the energy interval between E' and $E' + dE'$, then we can define the so-called *double differential cross section* by:

$$\frac{d^2\sigma}{d\Omega dE'} = \frac{n'}{jd\Omega dE'} \quad (2.4)$$

Here j refers to the incident beam flux in terms of particles per area and time. If we are not interested in the change of the energy of the radiation during the scattering process, or if our detector is not able to resolve this energy change, then we will describe the angular dependence by the so-called *differential cross section*:

$$\frac{d\sigma}{d\Omega} = \int_0^{\infty} \frac{d^2\sigma}{d\Omega dE'} dE' \quad (2.5)$$

Finally the so-called *total scattering cross section* gives us a measure for the total scattering probability independent of changes in energy and scattering angle:

$$\sigma = \int_0^{4\pi} \frac{d\sigma}{d\Omega} d\Omega \quad (2.6)$$

Therefore our task is to determine the arrangement of the atoms in the sample from the knowledge of the scattering cross section $d\sigma/d\Omega$. The relationship between scattered intensity and the structure of the sample is particularly simple in the so-called *Born approximation*, which is often also referred to as *kinematic scattering approximation*. In this case, refraction of the beam entering and leaving the sample, multiple scattering events and the extinction of the primary beam due to scattering within the sample are being neglected. Following Figure 2.3, the phase difference between a wave scattered at the origin of the coordinate system and at position \underline{r} is given by

$$\Delta\Phi = 2\pi \cdot \frac{(\overline{AB} - \overline{CD})}{\lambda} = \underline{k}' \cdot \underline{r} - \underline{k} \cdot \underline{r} = \underline{Q} \cdot \underline{r} \quad (2.7)$$

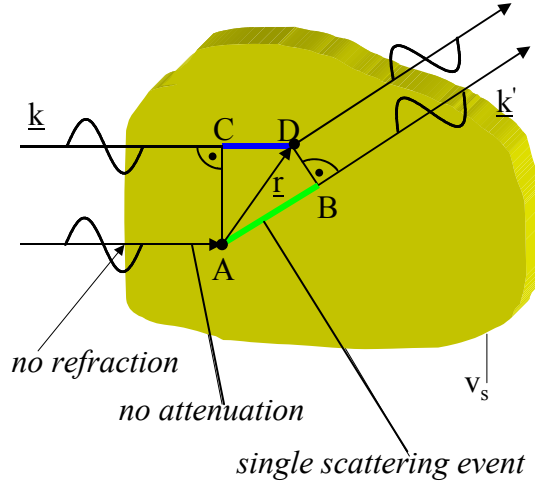


Fig. 2.3: A sketch illustrating the phase difference between a beam scattered at the origin of the coordinate system and a beam scattered at the position \underline{r} .

The scattered amplitude at the position \underline{r} is proportional to the scattering density $\rho_s(\underline{r})$ at this position. ρ_s depends on the type of radiation used and the interaction of this radiation with the sample. In fact, ρ_s is directly proportional to the interaction potential, as will be shown in the next chapter. Assuming a laterally coherent beam, the total scattering amplitude is given by a coherent superposition of the scattering from all points within the sample, i. e. by the integral

$$A = A_0 \cdot \int_{V_s} \rho_s(\underline{r}) \cdot e^{i\mathbf{Q}\cdot\underline{r}} d^3r \quad (2.8)$$

Here A_0 denotes the amplitude of the incident wave field. (2.8) demonstrates that the scattered amplitude is connected with the scattering density $\rho_s(\underline{r})$ by a simple Fourier transform. Knowledge of the scattering amplitude for all scattering vectors \underline{Q} allows us to determine via a Fourier transform the scattering density uniquely. This is the complete information on the sample, which can be obtained by the scattering experiment. Unfortunately, nature is not so simple. On one hand, there is the more technical problem that one is unable to determine the scattering cross section for all values of momentum transfer $\hbar\underline{Q}$. The more fundamental problem, however, is that normally the amplitude of the scattered wave is not measurable. Instead only the scattered intensity

$$I \sim |A|^2 \quad (2.9)$$

can be determined. Therefore the phase information is lost and the simple reconstruction of the scattering density via a Fourier transform is no longer possible. This is the so-called *phase problem* of scattering. There are ways to overcome the phase problem, e. g. by use of reference waves (e. g. holography). Then the scattering density becomes directly accessible. The question, which information we can obtain from a conventional scattering experiment despite the phase problem will be addressed below.

Which wavelength do we have to choose to obtain the required real space resolution? For information on a length scale L , a phase difference of about $\mathbf{Q}\cdot L \approx 2\pi$ has to be achieved. Otherwise according to (2.7) \underline{k}' and \underline{k} will not differ significantly. According to (2.3) $Q \approx 2\pi/\lambda$ for typical scattering angles ($2\theta \sim 60^\circ$). Combining these two estimates, we end up with the requirement that the wavelength λ has to be in the order of the real space length scale L under investigation. To give an example: with the wavelength in the order of 0.1 nm, atomic resolution can be achieved in a scattering experiment.

2.3 Fundamental scattering theory: The Born series

In this chapter, we will give a simple formulation of scattering theory. Our purpose is to derive (2.8) from fundamental principles. The conditions under which (2.8) holds and the limitations of kinematical scattering theory will thus become clearer. The derivation will be done for particle beams – in particular neutrons - for which the Schrödinger equation holds. Beginners can skip this chapter and continue with 2.4.

In quantum mechanics, neutrons are described as particle wave fields through the Schrödinger equation:

$$H\Psi = \left(-\frac{\hbar^2}{2m}\Delta + V \right) \Psi = i\hbar \frac{\partial}{\partial t} \Psi \quad (2.10)$$

ψ is the probability density amplitude, V the interaction potential. In case of purely elastic scattering $E = E'$, the time dependence can be described by the factor $\exp\left(-i\frac{E}{\hbar}t\right)$. Assuming this time dependence, a wave equation for the spatial part of the probability density amplitude ψ can be derived from (2.10):

$$\Delta\Psi + k^2(\underline{r})\Psi = 0 \quad (2.11)$$

In (2.11) we have introduced a spatially varying wave vector with the magnitude square:

$$k^2(\underline{r}) = \frac{2m}{\hbar^2}(E - V(\underline{r})) \quad (2.12)$$

Solutions of (2.10) in empty space (i. e. $V \equiv 0$) can be guessed immediately. They are given by plane waves $\Psi = \Psi_0 \exp\left[i\left(\underline{k} \cdot \underline{r} - \frac{E}{\hbar}t\right)\right]$ with $k^2 = \frac{2m}{\hbar^2}E$. The relations between magnitude of the wave vector k , wave length λ and energy of the neutron E can be written in practical units:

$$\begin{aligned} k[\text{\AA}^{-1}] &\approx 0.695\sqrt{E[\text{meV}]} \\ \lambda[\text{\AA}] &\approx 9.045/\sqrt{E[\text{meV}]} \\ E[\text{meV}] &\approx 81.8/\lambda^2[\text{\AA}] \end{aligned} \quad (2.13)$$

To give an example, neutrons of wavelength $\lambda = 2.4\text{\AA} = 0.24\text{nm}$ have an energy of 14.2 meV with a magnitude of the neutron wave vector of $k = 2.6\text{ \AA}^{-1}$.

To obtain solutions of the wave equation (2.11) in matter, we reformulate the differential equation by explicitly separating the interaction term:

$$(\Delta + k^2)\Psi = \frac{2m}{\hbar^2}V \cdot \Psi =: \chi \quad (2.14)$$

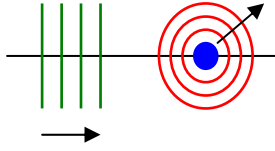
Here \underline{k} denotes the wave vector for propagation in empty space. The advantage of this formulation is that the solutions of the left hand side are already known. They are the plane waves in empty space. Equation (2.14) is a linear partial differential equation, i. e. the superposition principle holds: the general solution can be obtained as a linear combination of a complete set of solution functions. The coefficients in the series are determined by the boundary conditions. To solve (2.14) one can apply a method developed for inhomogeneous linear differential equations. For the moment, we assume that the right hand side is fixed (given as χ). We define a *Greens-function* by:

$$(\Delta + k^2)G(\underline{r}, \underline{r}') = \delta(\underline{r} - \underline{r}') \quad (2.15)$$

A solution of (2.15) is given by:

$$G(\underline{r}, \underline{r}') = \frac{e^{ik|\underline{r}-\underline{r}'|}}{4\pi|\underline{r}-\underline{r}'|} \quad (2.16)$$

The meaning of (2.16) is immediately clear: the scattering from a point-like scatterer (δ -potential) gives an emitted spherical wave. In a schematic graphical representation:

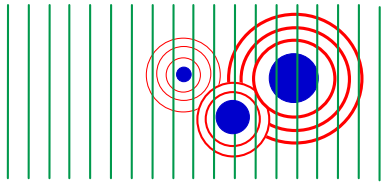


Using the Greens-function $G(\underline{r}, \underline{r}')$, we can write down a formal solution of the wave equation (2.14):

$$\Psi = \Psi^o + \int G(\underline{r}, \underline{r}') \chi(\underline{r}') d^3r' \quad (2.17)$$

Here, we have taken the initial conditions of an incident plane wave ψ^o into account. (2.17) is indeed a solution of (2.14) as can be easily verified by substituting (2.17) into (2.14). If we finally substitute the definition of χ , one obtains the so-called *Lippmann-Schwinger* equation:

$$\Psi(\underline{r}) = \psi^o(\underline{r}) + \frac{2m}{\hbar^2} \int G(\underline{r}, \underline{r}') V(\underline{r}') \Psi(\underline{r}') d^3r' \quad (2.18)$$



(2.18) has a simple interpretation: the incident plane wave $\psi^o(\underline{r})$ is superimposed by spherical waves emitted from scattering at positions \underline{r}' . The intensity of these spherical waves is proportional to the interaction potential $V(\underline{r}')$ and the amplitude of the wave field at the position \underline{r}' . To obtain the total scattering amplitude, we have to integrate over the entire sample volume V_s .

However, we still have not solved (2.14): our solution ψ appears again in the integral in (2.18). In other words, we have transformed differential equation (2.14) into an integral equation. The advantage is that for such an integral equation, a solution can be found by iteration. In the zeroth approximation, we neglect the interaction V completely. This gives $\psi = \psi^o$. The next higher order approximation for a weak interaction potential is obtained by substituting this solution in the right hand side of (2.18). The first non-trivial approximation can thus be obtained:

$$\Psi^1(\underline{r}) = e^{ik \cdot \underline{r}} + \frac{2m}{\hbar^2} \int \frac{\exp(ik|\underline{r}-\underline{r}'|)}{4\pi|\underline{r}-\underline{r}'|} V(\underline{r}') e^{ik \cdot \underline{r}'} d^3r' \quad (2.19)$$

(2.19) is nothing else but a mathematical formulation of the well-known *Huygens principle* for wave propagation.

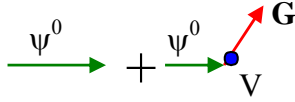
The approximation (2.19) assumes that the incident plane wave is only scattered once from the potential $V(\underline{r}')$. For a stronger potential and larger sample, multiple scattering processes will occur. Again, this can be deduced from the integral equation (2.18) by further iteration. For simplification we introduce a new version of equation (2.18) by writing the integral over the "Greens function" as operator \mathbf{G} :

$$\psi = \psi^o + \mathbf{G}V\psi \quad (2.20)$$

The so-called *first Born approximation*, which gives the *kinematical scattering theory* is obtained by substituting the wave function ψ on the right hand side by ψ^0 :

$$\psi^1 = \psi^o + \mathbf{G}V\psi^o \quad (2.21)$$

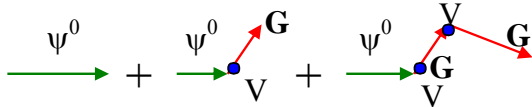
This first approximation can be represented by a simple diagram as a sum of an incident plane wave and a wave scattered once from the potential V :



The second approximation is obtained by substituting the solution of the first approximation (2.21) on the right hand side of equation (2.20):

$$\psi^2 = \psi^o + \mathbf{G}V\psi^1 = \psi^o + \mathbf{G}V\psi^o + \mathbf{G}V\mathbf{G}V\psi^o \quad (2.22)$$

Or in a diagrammatic form:



I. e. in the second approximation, processes are being taken into account, in which the neutron is scattered twice by the interaction potential V . In a similar manner, all higher order approximations can be calculated. This gives the so-called *Born series*.¹ For weak potential and small samples, this series converges rather fast. Often, the first approximation, the *kinematic scattering theory*, holds very well. This is especially the case for neutron scattering, where the scattering potential is rather weak, as compared to x-ray- or electron- scattering. Due to the strong Coulomb interaction potential, the probability for multiple scattering processes of electrons in solids is extremely high, making the interpretation of electron diffraction experiments very difficult. But even for neutrons, the kinematic scattering theory can break down, for example in the case of Bragg scattering from large ideally perfect single crystals, where the Born series does not converge. The wave equation has to be solved exactly under the boundary conditions given by the crystal geometry. For simple geometries, analytical solutions can be obtained. This is then called the *dynamical scattering theory*. Since for neutrons, the kinematical theory holds in most cases, or multiple scattering events can often be corrected for, we will no longer discuss dynamical theory in what follows and refer to [3, 6].

Let us return to the first Born approximation (2.19). In a further approximation, the Fraunhofer approximation, we assume that the size of the sample is significantly smaller than the distance sample-detector. The geometry to calculate the far field limit of (2.19) is given in Figure 2.4. Under the assumption $|R| \gg |r'|$, we can deduce from Figure 2.4 the following approximation for the emitted spherical wave:

$$\frac{\exp(ik|\underline{r}-\underline{r}'|)}{|\underline{r}-\underline{r}'|} \approx \frac{\exp(ik(R-\underline{r}' \cdot \hat{R}))}{R} \approx \frac{\exp(ikR)}{R} \cdot e^{-ik' \cdot r'} \quad (2.23)$$

The probability density amplitude for the scattered wave field in the limit of large distances from the sample is thus given by:

$$\Rightarrow \psi^1(R) = e^{ikR} + \frac{2m}{\hbar^2} \frac{e^{ikR}}{4\pi R} \int V(\underline{r}') e^{i\underline{Q} \cdot \underline{r}'} d^3r' \quad (2.24)$$

¹ Note that Born approximation or the Born series violates energy conservation: scattered waves are created without weakening of the incident plane wave. Born series can therefore only be applied in the limit of very weak scattering potentials.

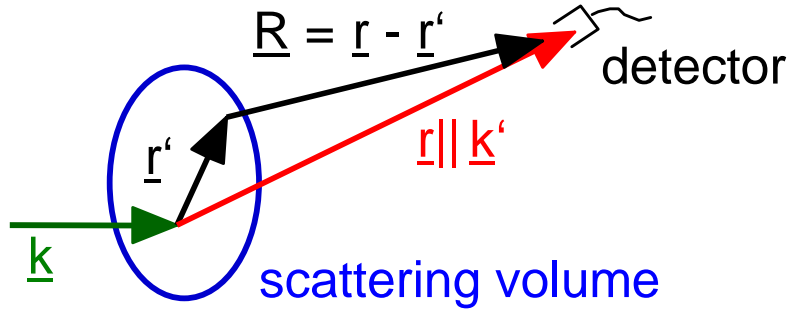


Fig. 2.4: Scattering geometry for the calculation of the far field limit at the detector. In the Fraunhofer approximation, we assume that $|\underline{R}| \gg |\underline{r}'|$.

This is just the sum of an incident plane wave and a spherical wave emitted from the sample as a whole. The amplitude of the scattered wave is given according to (2.24):

$$A(\underline{Q}) = \frac{m}{2\pi\hbar^2} \int V(\underline{r}) e^{i\underline{Q}\cdot\underline{r}} d^3r \sim F[V(\underline{r})] \quad (2.25)$$

The integral in the above equation is nothing but the transition matrix element of the interaction potential V between the initial and final plane wave states, therefore:

$$\frac{d\sigma}{d\Omega} = \left(\frac{m}{2\pi\hbar^2} \right)^2 |\langle \underline{k}' | V | \underline{k} \rangle|^2 \quad (2.26)$$

This formula corresponds to *Fermi's Golden Rule* from time-dependent perturbation theory, where the transition probability per time interval from state k to states k' is given by:

$$W_{k'k} = \frac{2\pi}{\hbar} |\langle k' | V | k \rangle|^2 \cdot \rho(E_{k'}) \quad (2.27)$$

Here, $\rho(E_{k'})$ denotes the density of states for the final states k' .

With this exact derivation of the scattering cross section, we can now deduce by comparison with (2.8) that the scattering density in the simple derivation of chapter 2.2 is just

$$\rho_s(\underline{r}) = \frac{m}{2\pi\hbar^2} V(\underline{r}) \text{ for particle beams governed by the Schrödinger equation.}$$

We now allow for inelastic processes, where the sample undergoes a change of its state from α to α' (α denotes a set of quantum numbers characterizing an eigenstate of the sample). In this case, due to the different length of the wavevectors for incoming and outgoing waves, we have to introduce factors k' and k , which arise from the density of states factor in (2.27). Since the scattering event must fulfill energy and momentum conservation, we arrive at the double differential cross section:

$$\frac{d^2\sigma}{d\Omega d\omega} = \frac{k'}{k} \left(\frac{m}{2\pi\hbar^2} \right)^2 \sum_{\alpha} p_{\alpha} \sum_{\alpha'} |\langle \underline{k}', \alpha' | V | \underline{k}, \alpha \rangle|^2 \cdot \delta(\hbar\omega + E_{\alpha} - E_{\alpha'}) \quad (2.28)$$

The first summation is carried out over all possible initial states α of the system, weighted with their thermodynamic occupation probability p_{α} . The sum over α' is the sum over all final states allowed by energy conservation, which is guaranteed through the δ -function. $\hbar\omega$ denotes the energy transfer of the neutron to the system. This double differential cross section will be discussed in the following lectures on inelastic scattering.

2.4 Coherence

In the above derivation, we assumed plane waves as initial and final states. For a real scattering experiment, this is an unphysical assumption. In the incident beam, a wave packet is produced by collimation (defining the direction of the beam) and monochromatization (defining the wavelength of the incident beam). Neither the direction \hat{k} , nor the wavelength λ have sharp values but rather have a distribution of finite width about their respective mean values. This wave packet can be described as a superposition of plane waves. As a consequence, the diffraction pattern will be a superposition of patterns for different incident wavevectors \underline{k} and the question arises, which information is lost due to these non-ideal conditions. This *instrumental resolution* is intimately connected with the *coherence* of the beam. Coherence is needed, so that the interference pattern is not significantly destroyed. Coherence requires a phase relationship between the different components of the beam. Two types of coherence can be distinguished.

- *Temporal or longitudinal coherence* due to a wavelength spread.

A measure for the longitudinal coherence is given by the length, on which two components of the beam with largest wavelength difference (λ and $\lambda + \Delta\lambda$) become fully out of phase.

According to the following figure, this is the case for $l_{\parallel} = n \cdot \lambda = \left(n - \frac{1}{2}\right)(\lambda + \Delta\lambda)$.

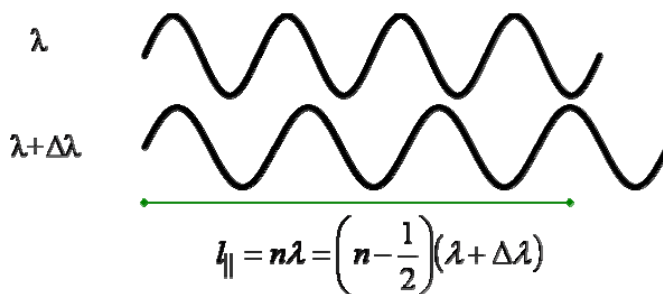


Fig. 2.5: A sketch illustrating the longitudinal coherence due to a wavelength spread.

From this, we obtain the *longitudinal coherence length* l_{\parallel} as

$$l_{\parallel} = \frac{\lambda^2}{2\Delta\lambda} \quad (2.29)$$

- *Transversal coherence* due to source extension

Due to the extension of the source (transverse beam size), the phase relation is destroyed for large source size or large divergence. According to the following figure, a first minimum occurs for

$$\frac{\lambda}{2} = d \cdot \sin \theta \approx d \cdot \theta.$$

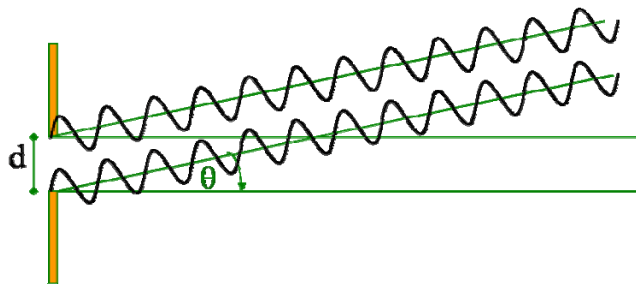


Fig. 2.6: A sketch illustrating the transversal coherence due to source extension.

From this, we obtain the *transversal coherence length* l_{\perp} as

$$l_{\perp} = \frac{\lambda}{2\Delta\theta} \quad (2.30)$$

Here $\Delta\theta$ is the divergence of the beam. Note that l_{\perp} can be different along different spatial directions: in many instruments, the vertical and horizontal collimations are different.

Together, the longitudinal and the two transversal coherence lengths (in two directions perpendicular to the beam propagation) define a *coherence volume*. This is a measure for a volume within the sample, in which the amplitudes of all scattered waves superimpose to produce an interference pattern. Normally, the coherence volume is significantly smaller than the sample size, typically a few 100 \AA for neutron scattering, up to μm for synchrotron radiation. Scattering between different coherence volumes within the sample is no longer coherent, i. e. instead of the amplitudes the intensities of the contributions to the scattering pattern have to be added. This limits the real space resolution of a scattering experiment to the extension of the coherence volume.

2.5 Pair correlation functions

After having clarified the conditions under which we can expect a coherent scattering process, let us now come back to the question, which information is accessible from the intensity distribution of a scattering experiment. From (2.9) we see that the phase information is lost during the measurement of the intensity. For this reason the Fourier transform of the scattering density is not directly accessible in most scattering experiments (note however that phase information can be obtained in certain cases).

Substituting (2.8) into (2.9) and applying variable substitution $\underline{R} = \underline{r}' - \underline{r}$, we obtain for the magnitude square of the scattering amplitude, a quantity directly accessible in a scattering experiment:

$$\begin{aligned} I &\sim \left| A(\underline{Q}) \right|^2 \sim \int d^3 r' \rho_s(\underline{r}') e^{i\underline{Q}\cdot\underline{r}'} \int d^3 r \rho_s^*(\underline{r}) e^{-i\underline{Q}\cdot\underline{r}} = \iint d^3 r' d^3 r \rho_s(\underline{r}') \rho_s^*(\underline{r}) e^{i\underline{Q}\cdot(\underline{r}'-\underline{r})} \\ &= \iint d^3 R d^3 r \rho_s(\underline{R}+\underline{r}) \rho_s^*(\underline{r}) e^{i\underline{Q}\cdot\underline{R}} \end{aligned} \quad (2.31)$$

This shows that the scattered intensity is proportional to the Fourier transform of a function $P(\underline{R})$:

$$I(\underline{Q}) \sim \int d^3 R P(\underline{R}) e^{i\underline{Q}\cdot\underline{R}} \quad (2.32)$$

This function denotes the so-called *Patterson function* in crystallography or more general the *static pair correlation function*:

$$P(\underline{R}) = \int d^3 r \rho_s^*(\underline{r}) \rho_s(\underline{r} + \underline{R}) \quad (2.33)$$

$P(\underline{R})$ correlates the value of the scattering density at position \underline{r} with the value at the position $\underline{r} + \underline{R}$, integrated over the entire sample volume. If, averaged over the sample, no correlation exists between the values of the scattering densities at position \underline{r} and $\underline{r} + \underline{R}$, then the Patterson function $P(\underline{R})$ vanishes. If, however, a periodic arrangement of a pair of atoms exists in the sample with a difference vector \underline{R} between the positions, then the Patterson function will have an extremum for this vector \underline{R} . Thus the Patterson function reproduces all the vectors connecting one atom with another atom in a periodic arrangement.

Quite generally, in a scattering experiment, pair correlation functions are being determined. In a coherent inelastic scattering experiment, we measure the *scattering law* $S(\underline{Q}, \omega)$, which is the

Fourier transform with respect to space and time of the spatial and temporal pair correlation function:

$$\frac{d^2\sigma}{d\omega d\Omega} \square S(\underline{Q}, \omega) = \frac{1}{2\pi\hbar} \int_{-\infty}^{+\infty} dt e^{-i\omega t} \int d^3r e^{i\underline{Q}\cdot\underline{r}} G(\underline{r}, t) \quad (2.34)$$

While the proportionality factor between the double differential cross section and the scattering law depends on the type of radiation and its specific interaction potential with the system studied, the spatial and temporal pair correlation function is only a property of the system studied and independent of the probe used:

$$G(\underline{r}, t) = \frac{1}{N} \sum_{ij} \int d^3r' \langle \delta(\underline{r}' - \underline{r}_j(0)) \cdot \delta(\underline{r}' + \underline{r} - \underline{r}_i(t)) \rangle = \frac{1}{N} \int d^3r' \langle \rho(\underline{r}', 0) \rho(\underline{r}' + \underline{r}, t) \rangle \quad (2.35)$$

Here, the pair correlation function is once expressed as a correlation between the position of N point-like particles (expressed by the delta functions) and once by the correlation between the densities at different positions in the sample for different times. In a magnetic system, we scatter from the atomic magnetic moments, which are vector quantities. Therefore, the scattering law becomes a tensor - the Fourier transform of the spin pair correlations:

$$\mathbf{S}^{\alpha\beta}(\underline{Q}, \omega) = \frac{1}{2\pi} \sum_l \int dt e^{i[\underline{Q}(\underline{R}_l - \underline{R}_0) - \omega t]} \langle S_0^\alpha(0) S_l^\beta(t) \rangle \quad (2.36)$$

α, β denote the Cartesian coordinates x, y, z ; \underline{R}_0 and \underline{R}_l are the spatial coordinates of a reference spin 0 and a spin l in the system.

2.6 Form-factor

So far we have not specified the nature of our sample. Now we assume an assembly on N scatterers of finite size, see Figure 2.7.

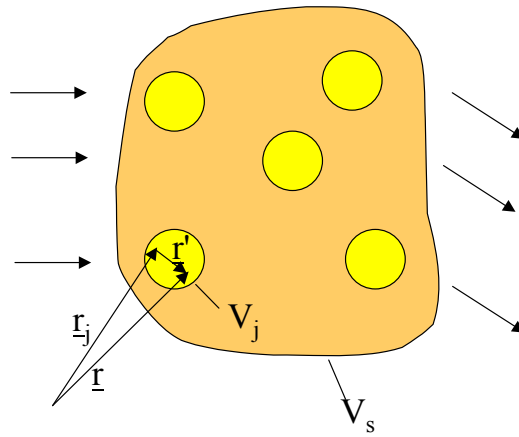


Fig. 2.7: Sketch showing the assembly of N scatterers of finite size and defining the quantities needed for the definition of the form factor.

These could be atoms in a solid or colloidal particles in a homogeneous solution. In what follows, we will separate the interference effects from scattering within one such a particle from the interference effects arising from scattering between different particles. With the decomposition of the vector \underline{r} into the centre-of-gravity-vector \underline{r}_j and a vector \underline{r}' within the particle, the scattering amplitude can be written as (all particles are assumed to be identical):

$$\begin{aligned}
A &\propto \int_{V_s} d^3r \rho_s(\underline{r}) e^{i\underline{Q}\cdot\underline{r}} = \sum_{j=1}^N \int_{V_j} d^3r \rho_s(\underline{r}) e^{i\underline{Q}\cdot\underline{r}} \\
&= \sum_{j=1}^N e^{i\underline{Q}\cdot\underline{r}_j} \int_{V_j^0} d^3r' \rho_s(\underline{r}') e^{i\underline{Q}\cdot\underline{r}'} =: \sum_{j=1}^N e^{i\underline{Q}\cdot\underline{r}_j} \rho_j^{tot} f_j(\underline{Q})
\end{aligned}
\tag{2.37}$$

With (2.37), we have separated the scattering from within the single particles from the interference between different particles. ρ_j^{tot} denotes the total scattering power of the particle. The *form-factor* $f(\underline{Q})$ is defined as the normalized amplitude of scattering from within one particle² (it describes the “form” of the particle):

$$f(\underline{Q}) \equiv \frac{\int_{V_j^0} d^3r' \rho_s(\underline{r}') e^{i\underline{Q}\cdot\underline{r}'}}{\int_{V_j^0} d^3r' \rho_s(\underline{r}')}
\tag{2.38}$$

For a homogeneous sphere

$$\rho_s(\underline{r}) = \begin{cases} 0 & |\underline{r}| > R \\ 1 & |\underline{r}| \leq R \end{cases}
\tag{2.39}$$

, the form-factor can be calculated by using spherical co-ordinates:

$$\Rightarrow f(Q) = 3 \cdot \frac{\sin QR - QR \cdot \cos QR}{(QR)^3}
\tag{2.40}$$

The function (2.40) is plotted in Figure 2.8. In forward direction, there is no phase difference between waves scattered from different volume elements within the sample (note: we assume the Fraunhofer approximation and work in a far field limit). The form-factor takes its maximum value of one. For finite scattering angles 2θ , the form-factor drops due to destructive interference from various parts within one particle and finally for large values of the momentum transfer shows damped oscillations around 0 as a function of QR .

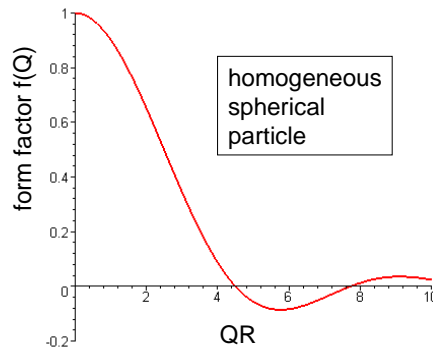


Fig. 2.8: Form-factor for a homogeneous sphere according to (2.40).

2.7 Scattering from a periodic lattice in three dimensions

As an example for the application of (2.8) and (2.9), we will now discuss the scattering from a three dimensional lattice of point-like scatterers. As we will see later, this situation corresponds to the scattering of thermal neutrons from a single crystal. More precisely, we will restrict ourselves to the case of a Bravais lattice with one atom at the origin of the unit cell. To

² For simplicity we now drop the index j

each atom we attribute a “scattering power³ α ”. The single crystal is finite with N , M and P periods along the basis vectors \underline{a} , \underline{b} and \underline{c} . The scattering density, which we have to use in (2.8) is a sum over δ -functions for all scattering centers:

$$\rho_s(\underline{r}) = \sum_{n=0}^{N-1} \sum_{m=0}^{M-1} \sum_{p=0}^{P-1} \alpha \cdot \delta(\underline{r} - (n \cdot \underline{a} + m \cdot \underline{b} + p \cdot \underline{c})) \quad (2.41)$$

The scattering amplitude is calculated as a Fourier transform:

$$A(\underline{Q}) \sim \alpha \sum_{n=0}^{N-1} e^{in\underline{Q} \cdot \underline{a}} \sum_{m=0}^{M-1} e^{im\underline{Q} \cdot \underline{b}} \sum_{p=0}^{P-1} e^{ip\underline{Q} \cdot \underline{c}} \quad (2.42)$$

Summing up the geometrical series, we obtain for the scattered intensity:

$$I(\underline{Q}) \sim |A(\underline{Q})|^2 = |\alpha|^2 \cdot \frac{\sin^2 \frac{1}{2} N\underline{Q} \cdot \underline{a}}{\sin^2 \frac{1}{2} \underline{Q} \cdot \underline{a}} \cdot \frac{\sin^2 \frac{1}{2} M\underline{Q} \cdot \underline{b}}{\sin^2 \frac{1}{2} \underline{Q} \cdot \underline{b}} \cdot \frac{\sin^2 \frac{1}{2} P\underline{Q} \cdot \underline{c}}{\sin^2 \frac{1}{2} \underline{Q} \cdot \underline{c}} \quad (2.43)$$

The dependence on the scattering vector \underline{Q} is given by the so-called *Laue function*, which factorizes according to the three directions in space. One factor along one lattice direction \underline{a} is plotted in Figure 2.9.

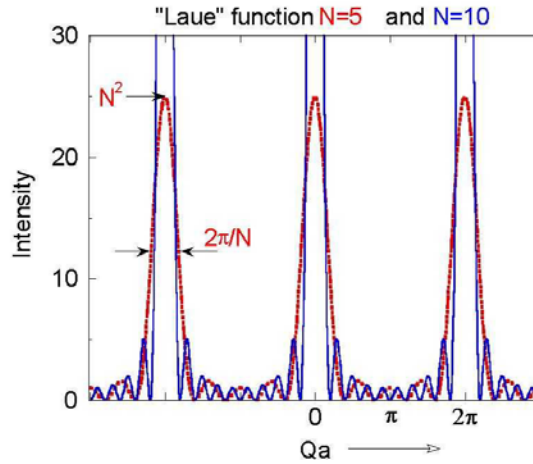


Fig. 2.9: Laue function along the lattice direction \underline{a} for a lattice with five and ten periods, respectively.

The main maxima occur at the positions $Q = n \cdot 2\pi/a$. The maximum intensity scales with the square of the number of periods N^2 , the half width is given approximately by $\Delta Q = 2\pi/(N \cdot a)$. The more periods contribute to coherent scattering, the sharper and higher are the main peaks. Between the main peaks, there are $N-2$ side maxima. With increasing number of periods N , their intensity becomes rapidly negligible compared to the intensity of the main peaks. The main peaks are of course the well known *Bragg reflections*, which we obtain for scattering from a crystal lattice. From the position of these Bragg peaks in momentum space, the metric of the unit cell can be deduced (lattice constants a , b , c and unit cell angles α , β , γ). The width of the Bragg peaks is determined by the size of the coherently scattering volume (parameters N , M , and P) - and some other factors for real experiments (resolution, mosaic distribution, internal strains, ...).

³ We will later see that this „scattering power“ is connected to the so-called scattering length of the atom.

2.8 Probes for scattering experiments in condensed matter science

In this chapter, we will discuss which type of radiation is suitable for condensed matter investigations. For neutron beams, we will then discuss the relevant interaction processes with matter in detail.

A list of requirements for the type of radiation used in condensed matter investigations looks as follows:

- (1) The achievable spatial resolution should be in the order of the inter-particle distances, which implies (see section 2.2) that the wavelength λ is in the order of the inter-particle distance L .
- (2) If we want to study volume effects, the scattering has to originate from the bulk of the sample, which implies that the radiation should be at most weakly absorbed within matter.
- (3) For a simple interpretation of the scattering data within the Born approximation (see section 2.2), multiple scattering effects should be negligible, i. e. the interaction of the radiation with matter should be weak.
- (4) For the sake of simplicity, the probe should have no inner degrees of freedom, which could be excited during the scattering process (i. e. avoid beams of molecules, which have internal vibrational or rotational degrees of freedom).
- (5) To study magnetic systems, we need a probe which interacts with the atomic magnetic moments in the sample.
- (6) If, in addition to structural studies, we want to investigate elementary excitations, we would like the energy of the probe to be in the order of the excitation energies, so that the energy change during the scattering process is easily measurable.

This list of requirements leads us to some standard probes in condensed matter research. First of all, electromagnetic radiation governed by the Maxwell equations can be used. Depending on the resolution requirements, we will use x-rays with wavelength λ of about 0.1 nm to achieve atomic resolution or visible light ($\lambda \sim 350 - 700 \text{ nm}$) to investigate e. g. colloidal particles in solution. Besides electromagnetic radiation, particle waves can be used. It turns out that thermal neutrons with a wavelength $\lambda \sim 0.1 \text{ nm}$ are particularly well adapted to the above list of requirements. The neutron beams are governed by the Schrödinger equation of quantum mechanics. An alternative is to use electrons, which for energies of around 100 keV have wavelengths in the order of 0.005 nm . As relativistic particles, they are governed by the Dirac equation of quantum mechanics. The big drawback of electrons as a condensed matter probe is the strong Coulomb interaction with the electrons in the sample. Therefore neither absorption, nor multiple scattering effects can be neglected. However the abundance of free electrons and the relative ease to produce optical elements makes them very suitable for imaging purposes (electron microscopy). Electrons, but also atomic beams are very powerful tools for surface science: due to their strong interaction with matter, both types of radiation are very surface sensitive. Low Energy Electron Diffraction LEED and Reflection High Energy Electron Diffraction RHEED are both used for in-situ studies of the crystalline structure during thin film growth, e.g. with Molecular Beam Epitaxy MBE. In what follows we will concentrate on neutron scattering as one of the probes, which is best suited for bulk studies on an atomic scale. We will introduce the properties of the neutron, discuss the absorption of neutrons in matter and derive the scattering cross sections for the main interaction processes with matter.

2.9 Properties of the neutron

We mentioned in the introduction that neutron beams provide a particularly useful probe for condensed matter investigations. The neutron is an elementary particle, a nucleon, consisting of three valence quarks, which are held together by gluons. It thus has an internal structure, which, however, is irrelevant for condensed matter physics, since the energy scales involved in its internal excitations are much too high. Keeping in mind the difference in lengths scales (diameter of an atom: about $0.1\text{nm}=10^{-10}\text{m}$; diameter of a neutron: about $1\text{fm}=10^{-15}\text{m}$), we can safely consider the neutron as a point-like particle without internal structure for our purposes. Due to the weak interaction, the neutron is not a stable particle. A free neutron undergoes a β -decay after an average lifetime of about 15 minutes:



This leaves ample time for scattering investigations. In contrast to the massless photon, the neutron has a mass m of about one atomic mass unit $\sim 1.675 \cdot 10^{-27}\text{ kg}$. The finite neutron mass is comparable to the mass of a nucleus and thus an appreciable amount of energy can be transferred during the scattering process. The neutron is a chargeless particle and thus does not show the strong Coulomb interaction with matter. This results in large penetration depths. Finally, the neutron has a nuclear spin $1/2$ giving rise to a magnetic dipolar moment of

$$\mu_n = \gamma \mu_N; \quad \gamma = 1.91; \quad \mu_N = 5.05 \cdot 10^{-27}\text{ J/T} \quad (2.45)$$

Due to this magnetic moment, the neutron can interact with the magnetic field of unpaired electrons in a sample leading to *magnetic scattering*. Thus magnetic structures and excitations can be studied by neutron scattering.

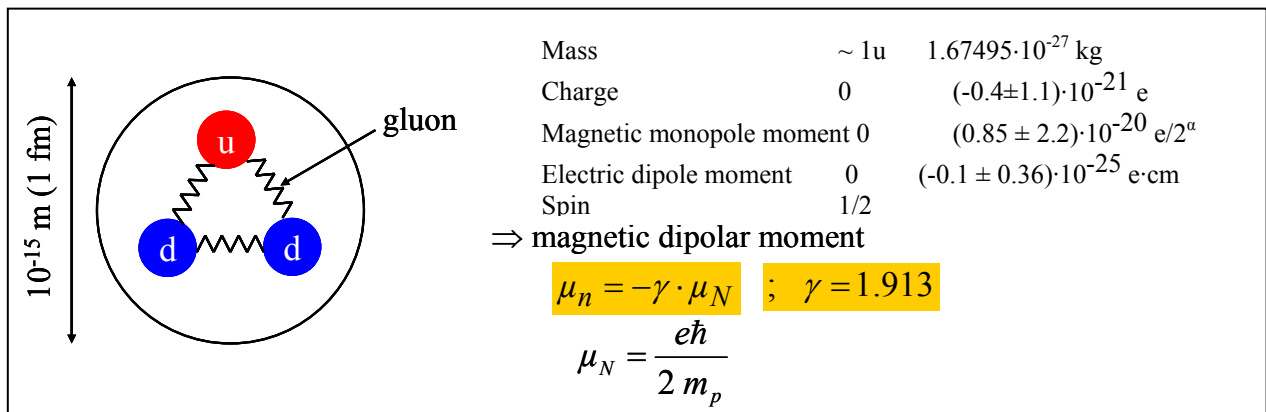


Fig. 2.10: Schematics of the neutron being composed of three quarks and gluons and the main quantities characterizing the neutron as a particle.

To calculate the interference effects during the scattering process, a neutron has to be described as a matter wave with momentum

$$\underline{p} = m \cdot \underline{v} = \hbar \underline{k}; \quad p = h / \lambda \quad (2.46)$$

and energy

$$E = \frac{1}{2} m v^2 = \frac{\hbar^2 k^2}{2m} = \frac{h^2}{2m\lambda^2} \equiv k_B T_{eq} \quad (2.47)$$

Here \underline{v} is the velocity of the neutron and T_{eq} defines the temperature equivalent of the kinetic energy of the neutron. In practical units:

$$\lambda[nm] = \frac{400}{v[m/s]} \quad (2.48)$$

$$E[meV] = \frac{0.818}{\lambda^2[nm]}$$

Let us consider the example of so-called *thermal neutrons* from a moderator at ambient temperature corresponding to a temperature equivalent of $T_{eq} \sim 300K$. According to (2.47), their wavelength is $0.18nm$, matching perfectly the distance between atoms. The energy of thermal neutrons is around $25meV$, which matches well the energy of elementary excitations, such as spin waves (magnons) or lattice vibrations (phonons). Together with the usually large penetration depths (charge = 0) and the magnetic interaction, these properties make neutrons so extremely useful for condensed matter investigations.

In the elementary scattering theory of chapter 2.3, we saw that the relevant quantity is the interaction potential $V(\underline{r})$ of the probe with the system from which the probe is scattered. This potential enters in the cross-section in kinematical theory derived either from Born approximation or from Fermi's golden rule. To determine this interaction potential, we will look in more detail at the interaction of neutrons with matter. For neutrons there exist two dominant interactions: the interaction of the neutron with nuclei and its interaction with the magnetic field in the sample. The nuclear interaction results from the so-called strong interaction of particle physics, which is also responsible for the binding of neutrons and protons in the atomic nuclei. The interaction with the magnetic field is nothing but the magnetic dipole interaction of the neutron due to its dipolar moment with the magnetic field of unpaired electrons. There are other interactions, which are significantly weaker. One is the interaction of the neutron with the electric fields in the sample due to the neutrons magnetic dipole moment. This is a purely relativistic effect. Another is the magnetic dipole interaction of the neutron with the magnetic field produced by the nuclei. Since such interactions are several orders of magnitude weaker than the nuclear and magnetic interaction, they can usually be neglected and we will not discuss them further in this lecture.

2.10 Nuclear interaction: Scattering and absorption

To evaluate the cross section (2.26) for nuclear scattering, we have to specify the interaction potential with the nucleus. To derive this interaction potential from first principles is one of the fundamental challenges of nuclear physics. Fermi has proposed a phenomenological potential based on the argument that the wavelength of thermal neutrons is much larger than the nuclear radius. This means that the nuclei are point-like scatterers which leads to isotropic, Q-independent, (so-called s-wave) scattering. We will therefore use the so-called *Fermi-pseudopotential*:

$$V(\underline{r}) = \frac{2\pi\hbar^2}{m} b\delta(\underline{r} - \underline{R}) \quad (2.49)$$

to evaluate the cross section (2.26).

Note, that despite the fact that the strong interaction of high energy physics is responsible for the scattering of the neutron with the nucleus, the scattering probability is small due to the small nuclear radius. Therefore, we can apply the first Born approximation. The quantity b introduced in (2.49) is a phenomenological quantity describing the strength of the interaction potential and is referred to as the *scattering length*. Tabulated values of b can be found in [7] or at <http://www.ncnr.nist.gov/resources/n-lengths/>. The total cross section of a given nucleus

is $\sigma = 4\pi|b|^2$, corresponding to the surface area of a sphere with radius b . Since the interaction potential obviously depends on the details of the nuclear structure, b is different for different isotopes of the given element and also for different nuclear spin states. This fact gives rise to the appearance of so-called *coherent* and *incoherent scattering*, see section 2.12. Figure 2.11 shows the variation of the scattering amplitude as a function of atomic weight throughout the periodic table. The scattering length is mostly positive but can also adopt negative values. Since $-1 = \exp(i\pi)$ this negative sign corresponds to a phase shift of π (or 180°) during the scattering process. The scattering length roughly follows the dashed line labeled *potential scattering contribution*, despite the fact that there are rather large excursions from this line.

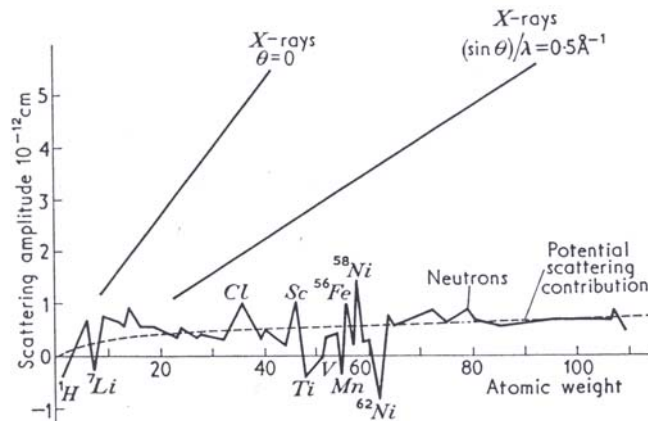


Fig. 2.11: Scattering length as a function of atomic weight throughout the periodic table (from *Research, London* 7 (1954), 257).

In the simplest one dimensional model, we can describe the nucleus as a rectangular potential well, see Figure 2.12.

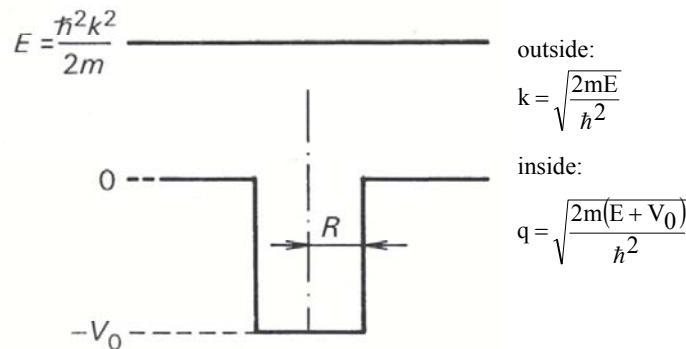


Fig. 2.12: The nucleus described as a potential well of radius R and depth $-V_0$, while the neutron has the kinetic energy $E = \frac{\hbar^2 k^2}{2m}$.

The wave function of the neutron being scattered from such a potential well can be written as:

$$\Psi(r) \sim e^{ikr} + \frac{f}{r} e^{ikr} \quad (2.50)$$

Here the first term describes the incident plane wave and the second term describes a spherical wave emitted from the nucleus. f describes the scattering amplitude. In the limit of a hard sphere, the wave function on the surface of the nucleus has to vanish since the neutron cannot penetrate inside the hard sphere. Mathematically this is described by the condition $\psi(R) = 0$ or $-f = R$. The scattering length is defined as $b = -f$, so that its value is positive for

most nuclei. Therefore for pure potential scattering, where the nucleus is assumed to be a hard sphere, b attains the value of the nuclear radius $b = R$, which is plotted in Figure 2.11 as a dashed line: the *potential scattering* contribution. The marked deviations from this overall behavior are due to so-called *resonance scattering*. In a simplified picture, such resonances occur, when the neutron energy is such that absorption of the neutron in the nucleus produces a bound excited state. This can lead to a resonant absorption process, but it can also lead to resonance scattering, a typical second order perturbation process: in the initial state, the nucleus is in its ground state and the interaction with the neutron can be described as a virtual transition into an excited state of the compound nucleus and back with a re-emission of the neutron, where the nucleus decays back from the excited compound system into its ground state. This process $n+K \rightarrow C^* \rightarrow K+n$ has a cross-section given by the famous *Breit-Wigner-formula*:

$$\sigma_R = 4\pi \left| R + \frac{\text{const}}{E - E_R + \frac{1}{2}i\Gamma} \right|^2 \quad (2.51)$$

Here R is the radius of the nucleus, E the neutron energy, E_R the resonance energy and Γ a damping term connected with the life-time of the excited state. As one can see, this formula describes very strong energy dependence with a pronounced maximum, when the neutron energy equals the resonance energy. Moreover, the resonance amplitude has an imaginary part, which describes the *resonance absorption*. In the resonant absorption process, the neutron is captured by the nucleus, leading to a compound nucleus in an excited state, containing one more neutron than the original nucleus. In a subsequent nuclear reaction, the compound nucleus gets rid of its excess energy. Examples for such absorption reactions will be given in the subsequent section. Finally the Breit-Wigner-formula gives an indication that the scattering length can be negative whenever the resonant term is negative (i. e. $E < E_R$), and its magnitude is larger than the contribution from potential scattering.

2.11 Neutron absorption

As explained above, neutron absorption can occur during nuclear reactions. Far away from the resonance, the absorption cross section is given by

$$\sigma_a \sim \lambda \sim \frac{1}{v} \quad (2.52)$$

This proportionality to the wavelength λ or the inverse velocity $1/v$ is a result of the density of states appearing in Fermi's golden rule. One can argue that wavelength and neutron velocity v are inversely proportional and thus, for longer wavelength i. e. smaller velocity, the neutron remains correspondingly longer close to the nucleus, which leads to a higher absorption cross-section. Table 2.1 gives examples for neutron absorption processes connected with nuclear reactions.

<u>Examples:</u>		
σ_a (25 meV) [barn]		
5333	$n + {}^3\text{He} \rightarrow {}^4\text{He}^* \rightarrow p + {}^3\text{T}$	} neutron detection
940	$n + {}^6\text{Li} \rightarrow {}^7\text{Li}^* \rightarrow {}^3\text{T} + {}^4\text{He}$	
3837	$n + {}^{10}\text{B} \rightarrow {}^{11}\text{B}^* \rightarrow {}^4\text{He} + {}^7\text{Li} + \gamma$	
681	$n + {}^{235}\text{U} \rightarrow \text{fission}$	

Tab. 2.1: Examples for neutron absorption processes due to nuclear reactions. The absorption cross-section is given for neutrons of energy 25 meV in barn = $10^{-28} \text{ m}^2 = 100 \text{ fm}^2$.

As an example, there is a high probability of neutrons to be absorbed by ^3He nuclei, because the ^4He or α -particle is very stable, since it corresponds to a closed nuclear shell. However, during the absorption of the neutron, the ^4He nucleus is produced in an excited state. It gets rid of its surplus energy by decay into a proton and a triton⁴ ^3T . Since these two particles have very high energies of about 0.5 MeV due to the nuclear reaction, charged particles are created during this decay, which can be used for neutron detection in a proportional counter. In a similar manner, the reaction with ^6Li , ^{10}B or ^{235}U can be used to build neutron detectors. It should be mentioned, however, that the neutron absorption in ^3He is very strongly dependent on the relative orientation of the nuclear spins of both particles. While for anti parallel spin direction, the absorption cross-section is ≈ 6000 barn, it reduces to 2 barn for parallel spin direction. This effect can be used to build efficient neutron polarization filters. By optical pumping with laser light, the nuclear moment of the ^3He nuclei can be aligned along one direction (so-called hyperpolarized ^3He gas). If an unpolarized neutron beam passes a filter cell filled with hyperpolarized ^3He , the neutrons with spin moment anti parallel to the nuclear moment of the ^3He have a high probability to be absorbed, while neutrons with the other spin direction have a high probability to be transmitted. For an appropriate thickness of the filter cell, a very high neutron beam polarization can be achieved in this manner.

Another class of absorption processes are so-called (n, γ) -resonances. Examples are given in Table 2.2. In these processes, a nucleus is produced, which contains one additional neutron and this compound nucleus decays into the ground state by emission of γ -radiation. Prominent (n, γ) -resonances occur for Cadmium or Gadolinium where, depending on the isotope, the absorption cross-section can be very high, see Table 2.2. These metals are often used as neutron absorbers in shieldings or diaphragms, which define the size of the neutron beam. One should, however, be aware that in these reactions, γ -radiation of very high energy is being released, which requires additional lead shielding for radiation protection.

	nucleide	σ_γ [barn]	$E_{\text{resonance}}$ [meV]
(n, γ)-resonances:	^{113}Cd	20600	178
	^{151}Eu	9200	321
	^{155}Gd	60900	26.8
	^{157}Gd	254000	31.4

Tab. 2.2: Examples for (n, γ) -resonances with the cross-section in barn and the resonance energy in meV.

As described by the Breit-Wigner-Formula, these resonance absorption cross-sections have very strong energy dependences. The simple proportionality to the wavelength given in equation (2.52) no longer holds close to the resonance energies. As an example, we show the energy dependence of the absorption cross-section for Cadmium in Figure 2.13. Such data can be found in the compilation [8].

⁴ The triton ^3T nucleus is a hydrogen isotope with one proton and 2 neutrons.

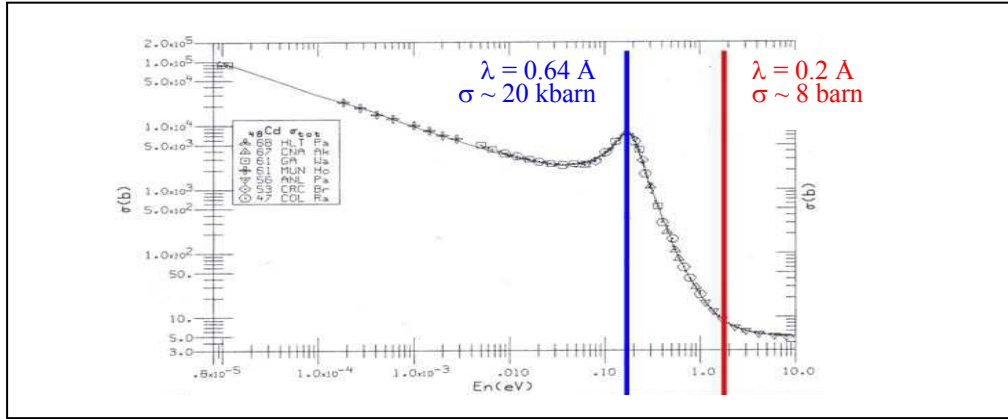


Fig. 2.13: Absorption cross-section of the element Cadmium as a function of energy in a double logarithmic representation (from 8).

Figure 2.13 shows that for lower energies, i. e. long wavelengths, the proportionality of the absorption cross-section to the wavelength holds to very good approximation. However, there is a strong resonance for a wavelength of 0.64 Å, where the cross-section attains a maximum of about 20 kbarn. Above this energy, i. e. for shorter wavelengths, the absorption cross-section drops drastically. At a wavelength of 0.2 Å, it attains a value of only 8 barn. This shows that in the thermal energy range, Cadmium can be used as an efficient neutron absorber. However, one has to be careful and not use it for the same purpose in case of hot neutrons, where Cadmium becomes virtually transparent. There are many more resonances for higher neutron energies, which are not relevant for neutron scattering, where only hot, thermal and cold neutrons are being used.

A similar strong energy dependence occurs for the element Gadolinium. Usually, neutron scatterers try to avoid samples containing Gadolinium since it is the most absorbing element, especially the isotope ^{157}Gd . However, the resonances lay right in the thermal neutron energy range. If the scattering experiment is performed with hot neutrons, the absorption cross-section of Gadolinium becomes much smaller and scattering experiments become feasible⁵.

2.12 Coherent and incoherent scattering

As mentioned above, the nuclear interaction potential depends on the details of the nuclear structure and thus, the scattering length b is different for different isotopes of a given element and also for different nuclear spin states. In this section, we will discuss the effects of these special properties of the interaction of neutrons and nuclei for the scattering from condensed matter.

Let us assume an arrangement of atoms with scattering lengths b_i on fixed positions \underline{R}_i . For this case, the scattering potential writes:

$$V(\underline{r}) = \frac{2\pi\hbar^2}{m_n} \sum_i b_i \delta(\underline{r} - \underline{R}_i) \quad (2.53)$$

The scattering amplitude is obtained from a Fourier transform:

⁵ Another possibility is to use isotope enriched Gadolinium. While the isotope ^{157}Gd with natural abundance 15.7% has a thermal absorption cross section of 259000 barn, the isotope ^{158}Gd , which is the most abundant with 24.8%, and has an absorption cross section of only 2.2 barn.

$$A(\underline{Q}) = \sum_i b_i e^{i\underline{Q} \cdot \underline{R}_i} \quad (2.54)$$

When we calculate the scattering cross section, we have to take into account that the different isotopes are distributed randomly over all sites. Also the nuclear spin orientation is random, except for very low temperatures in external magnetic fields. Therefore, we have to average over the random distribution of the scattering length in the sample:

$$\frac{d\sigma}{d\Omega}(\underline{Q}) \sim |A(\underline{Q})|^2 = \left\langle \sum_i b_i e^{i\underline{Q} \cdot \underline{R}_i} \cdot \sum_j b_j^* e^{-i\underline{Q} \cdot \underline{R}_j} \right\rangle \quad (2.55)$$

In calculating the expectation value of the product of the two scattering lengths at sites i and j , we have to take into account that according to the above assumption, the distribution of the scattering length on the different sites is completely uncorrelated. This implies that for $i \neq j$, the expectation value of the product equals to the product of the expectation values. Only for $i = j$ a correlation occurs, which gives an additional term describing the mean quadratic deviation from the average:

$$\langle b_i b_j \rangle = \begin{cases} \langle b \rangle \langle b \rangle = \langle b \rangle^2 & i \neq j \\ \langle b^2 \rangle = \langle b \rangle^2 + \langle (b - \langle b \rangle)^2 \rangle & i = j \end{cases}$$

The line for $i = j$ results from the identity:

$$\langle (b - \langle b \rangle)^2 \rangle = \langle b^2 - 2b\langle b \rangle + \langle b \rangle^2 \rangle = \langle b^2 \rangle - \langle b \rangle^2 \quad (2.56)$$

Therefore, we can write the cross section in the following form:

$$\begin{aligned} \frac{d\sigma}{d\Omega}(\underline{Q}) &= \langle b \rangle^2 \left| \sum_i e^{i\underline{Q} \cdot \underline{R}_i} \right|^2 && \text{"coherent"} \\ &+ N \langle (b - \langle b \rangle)^2 \rangle && \text{"incoherent"} \end{aligned} \quad (2.57)$$

The scattering cross section is as a sum of two terms. Only the first term contains the phase factors $e^{i\underline{Q} \cdot \underline{R}}$, which result from the coherent superposition of the scattering from pairs of scatterers. This term takes into account interference effects and is therefore named *coherent scattering*. The scattering length averaged over the isotope- and nuclear spin- distribution enters this term. The second term in (2.57) does not contain any phase information and is proportional to the number N of atoms (and not to N^2 !). This term is not due to the interference of scattering from different atoms. As we can see from (2.56) (line $i = j$), this term corresponds to the scattering from single atoms, which subsequently superimpose in an incoherent manner (adding intensities, not amplitudes!). This is the reason for the intensity being proportional to the number N of atoms. Therefore the second term is called *incoherent scattering*. Coherent and incoherent scattering are illustrated in Figure 2.14.

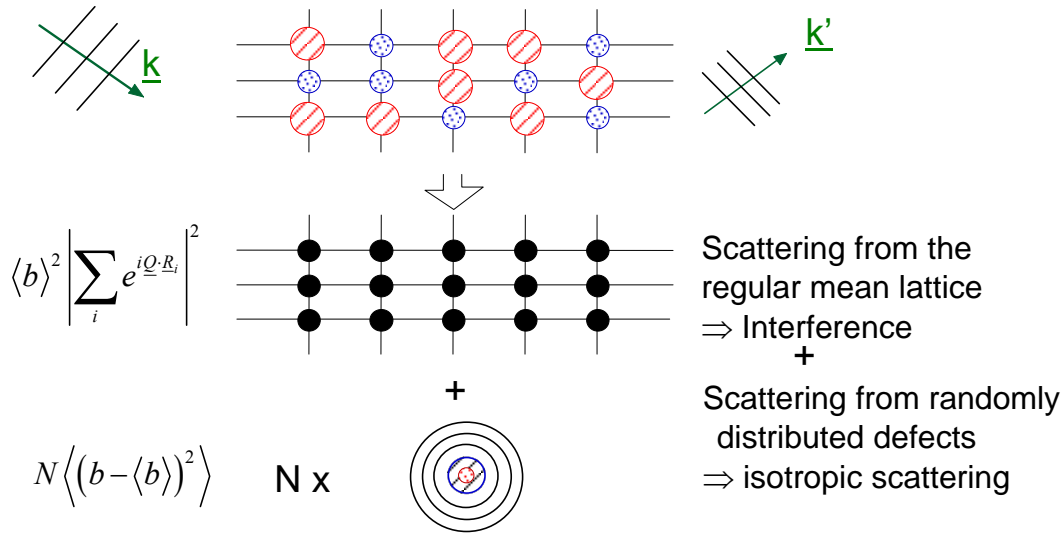


Fig. 2.14: Two-dimensional schematic illustration of the scattering process from a lattice of N atoms of a given chemical species, for which two isotopes (small dotted circles and large hatched circles) exist. The area of the circle represents the scattering cross section of the single isotope. The incident wave (top part of the figure for a special arrangement of the isotopes) is scattered coherently only from the average structure. This gives rise to Bragg peaks in certain directions. In the coherent scattering only the average scattering length is visible. Besides these interference phenomena, an isotropic background is observed, which is proportional to the number N of atoms and to the mean quadratic deviation from the average scattering length. This incoherent part of the scattering is represented by the lower part of the figure.

The most prominent example for *isotope incoherence* is elementary nickel. The scattering lengths of the nickel isotopes are listed together with their natural abundance in Table 2.3 [7]. The differences in the scattering lengths for the various nickel isotopes are enormous. Some isotopes even have negative scattering lengths. This is due to resonant bound states, as compared to the usual potential scattering.

Isotope	Natural Abundance	Nuclear Spin	Scattering Length [fm]
^{58}Ni	68.27 %	0	14.4(1)
^{60}Ni	26.10 %	0	2.8(1)
^{61}Ni	1.13 %	$3/2$	7.60(6)
^{62}Ni	3.59 %	0	-8.7(2)
^{64}Ni	0.91 %	0	-0.37(7)
Ni			10.3(1)

Tab. 2.3: The scattering lengths of the nickel isotopes and the resulting scattering length of natural ^{28}Ni [7].

Neglecting the less abundant isotopes ^{61}Ni and ^{64}Ni , the average scattering length is calculated as:

$$\langle b \rangle \approx [0.68 \cdot 14.4 + 0.26 \cdot 2.8 + 0.04 \cdot (-8.7)] \text{fm} \approx 10.2 \text{fm} \quad (2.58)$$

, which gives the total coherent cross section of:

$$\Rightarrow \sigma_{\text{coherent}} = 4\pi \langle b \rangle^2 \approx 13.1 \text{ barn (exact : 13.3(3) barn)} \quad (2.59)$$

The incoherent scattering cross section per nickel atoms is calculated from the mean quadratic deviation:

$$\sigma_{incoherent}^{Isotope} = 4\pi \left[0.68 \cdot (14.4 - 10.2)^2 + 0.26 \cdot (2.8 - 10.2)^2 + 0.04 \cdot (-8.7 - 10.2)^2 \right] fm^2 \quad (2.60)$$

$$\approx 5.1barn \text{ (exact : } 5.2(4)barn)$$

Values in parentheses are the exact values taking into account the isotopes ^{61}Ni and ^{64}Ni and the nuclear spin incoherent scattering (see below). From (2.59) and (2.60), we learn that the incoherent scattering cross section in nickel amounts to more than one third of the coherent scattering cross section.

The most prominent example for *nuclear spin incoherent scattering* is elementary hydrogen. The nucleus of the hydrogen atom, the proton, has the nuclear spin $I = \frac{1}{2}$. The total nuclear spin of the system H + n can therefore adopt two values: $J = 0$ and $J = 1$. Each state has its own scattering length: b_- for the singlet state ($J = 0$) and b_+ for the triplet state ($J = 1$) - compare Table 2.4.

Total Spin	Scattering Length	Abundance
J = 0	$b_- = -47.5 \text{ fm}$	$\frac{1}{4}$
J = 1	$b_+ = 10.85 \text{ fm}$	$\frac{3}{4}$
$\langle b \rangle = -3.739(1) \text{ fm}$		

Tab. 2.4: Scattering lengths for hydrogen [7].

As in the case of isotope incoherence, the average scattering length can be calculated:

$$\langle b \rangle = \left[\frac{1}{4}(-47.5) + \frac{3}{4} \cdot (10.85) \right] fm = -3.74 fm \quad (2.61)$$

This corresponds to a coherent scattering cross section of about $\approx 1.76 \text{ barn}$ [7]:

$$\Rightarrow \sigma_{coherent} = 4\pi \langle b \rangle^2 = 1.7568(10) barn \quad (2.62)$$

The nuclear spin incoherent part is again given by the mean quadratic deviation from the average:

$$\sigma_{incoherent}^{nuclear\ spin} = 4\pi \left[\frac{1}{4}(-47.5 + 3.74)^2 + \frac{3}{4}(10.85 + 3.74)^2 \right] fm^2 = 80.2 barn$$

$$\text{(exact: } 80.26(6) barn) \quad (2.63)$$

Comparing (2.62) and (2.63), it is immediately clear that hydrogen scatters mainly incoherently. As a result, we observe a large background for all samples containing hydrogen. We should avoid all hydrogen containing glue for fixing our samples to a sample stick. Finally, we note that deuterium with nuclear spin $I = 1$ has a much more favorable ratio between coherent and incoherent scattering:

$$\sigma_{coh}^D = 5.592(7)barn; \quad \sigma_{inc}^D = 2.05(3)barn \quad (64)$$

The coherent scattering lengths of hydrogen (-3.74 fm) and deuterium (6.67 fm) are significantly different. This can be used for contrast variation by isotope substitution in all samples containing hydrogen, i. e. in biological samples or soft condensed matter samples, see corresponding chapters.

A further important element, which shows strong nuclear incoherent scattering, is vanadium. Natural vanadium consists to 99,75 % of the isotope ^{51}V with nuclear spin 7/2. By chance, the

ratio between the scattering lengths b_+ and b_- of this isotope are approximately equal to the reciprocal ratio of the abundances. Therefore, the coherent scattering cross section is very small and the incoherent cross section dominates [7]:

$$\sigma_{coh}^V = 0.01838(12) \text{ barn}; \quad \sigma_{incoh}^V = 5.08(6) \text{ barn} \quad (2.65)$$

For this reason, Bragg scattering of vanadium is difficult to observe above the large incoherent background. However, since incoherent scattering is isotropic, the scattering from vanadium can be used to calibrate multi-detector arrangements.

Here, we will not discuss scattering lengths for further elements and refer to the values tabulated in [7].

2.13 Magnetic neutron scattering

So far, we have only discussed the scattering of neutrons by the atomic nuclei. Apart from nuclear scattering, the next important process is the scattering of neutrons by the magnetic field created within the sample from the moments of unpaired electrons. This so-called magnetic neutron scattering comes about by the magnetic dipole-dipole interaction between the magnetic dipole moment of the neutron and the magnetic field of the unpaired electrons, which has spin and orbital angular momentum contributions. This magnetic neutron scattering allows us to study the magnetic properties of a sample on an atomic level, i. e. with atomic spatial- and atomic energy- resolution. In what follows, we will give an introduction into the formalism of magnetic neutron scattering, restricting ourselves to the case of elastic magnetic scattering. Inelastic magnetic scattering will be discussed in subsequent lectures.

To derive the magnetic scattering cross section of thermal neutrons, we consider the situation shown in Figure 2.15: a neutron with the nuclear moment μ_n is at position \underline{R} with respect to an electron with spin \underline{S} , moving with a velocity \underline{v}_e .

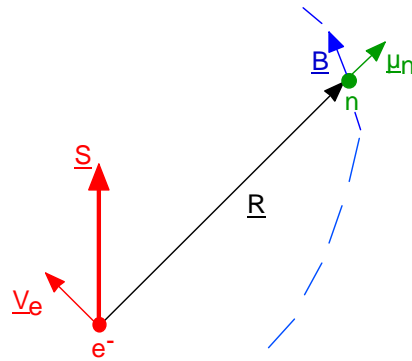


Fig. 2.15: Geometry for the derivation of the interaction between neutron and electron.

Due to its magnetic dipole moment, the neutron interacts with the magnetic field of the electron according to (“Zeeman-potential”):

$$\mathbf{V}_m = -\underline{\mu}_n \cdot \underline{B} \quad (2.66)$$

Here, the magnetic moment of the neutron is given by:

$$\underline{\mu}_n = -\gamma_n \mu_N \cdot \underline{\sigma} \quad (2.67)$$

$\underline{\sigma}$ denotes the spin operator, μ_N the nuclear magneton and $\gamma_N = -1.913$ the gyromagnetic factor of the neutron. The magnetic field \underline{B} of an electron is due to a spin- and orbital- part $\underline{B} = \underline{B}_S + \underline{B}_L$. The dipole field of the spin moment is given by:

$$\underline{B}_s = \nabla \times \left(\frac{\underline{\mu}_e \times \underline{R}}{R^3} \right) ; \quad \underline{\mu}_e = -2\mu_B \cdot \underline{S} \quad (2.68)$$

The field due to the movement of the electron is given according to Biot-Savart:

$$\underline{B}_L = \frac{-e}{c} \frac{\underline{v}_e \times \underline{R}}{R^3} \quad (2.69)$$

The magnetic scattering cross section for a process, where the neutron changes its wave vector from \underline{k} to \underline{k}' and the projection of its spin moment to a quantization axis z from σ_z to σ_z' can be expressed within the first Born approximation:

$$\frac{d\sigma}{d\Omega} = \left(\frac{m_n}{2\pi\hbar^2} \right)^2 \left| \langle \underline{k}' \sigma_z' | \underline{V}_m | \underline{k} \sigma_z \rangle \right|^2 \quad (2.70)$$

As mentioned, we only consider the single differential cross section for elastic scattering. Introducing the interaction potential from (2.66) to (2.69) in (2.70) we obtain after some algebra [1, 4]:

$$\frac{d\sigma}{d\Omega} = (\gamma_n r_0)^2 \left| -\frac{1}{2\mu_B} \langle \sigma_z' | \underline{\sigma} \cdot \underline{M}_\perp(\underline{Q}) | \sigma_z \rangle \right|^2 \quad (2.71)$$

The pre-factor $\gamma_n r_0$ has the value $\gamma_n r_0 = 0.539 \cdot 10^{-12} \text{ cm} = 5.39 \text{ fm}$. Here, $\underline{M}_\perp(\underline{Q})$ denotes the component of the Fourier transform of the sample magnetization, which is perpendicular to the scattering vector \underline{Q} (see Figure 2.16):

$$\underline{M}_\perp(\underline{Q}) = \hat{\underline{Q}} \times \underline{M}(\underline{Q}) \times \hat{\underline{Q}} \quad (2.72)$$

$$\underline{M}(\underline{Q}) = \int \underline{M}(\underline{r}) e^{i\underline{Q} \cdot \underline{r}} d^3 r \quad (2.73)$$

The total magnetization is given as a sum of the spin- and orbital-angular- momentum part according to:

$$\begin{aligned} \underline{M}(\underline{r}) &= \underline{M}_S(\underline{r}) + \underline{M}_L(\underline{r}) \\ \underline{M}_S(\underline{r}) &= -2\mu_B \cdot \underline{S}(\underline{r}) = -2\mu_B \sum_i \delta(\underline{r} - \underline{r}_i) \underline{S}_i \end{aligned} \quad (2.74)$$

(2.71) tells us that with magnetic neutron scattering, we are able to determine the magnetization $\underline{M}(\underline{r})$ in microscopic atomic spatial co-ordinates \underline{r} . This gives a lot more information than a simple macroscopic measurement, where we obtain the ensemble average of the magnetization over the entire sample. We also see from (2.71) that the orientation of the nuclear spin momentum of the neutron (represented by σ_z) plays an important role in magnetic scattering. This is not surprising, since magnetism is a vector property of the sample and obviously there should be an interaction with the vector property of the neutron, its nuclear magnetic moment. Therefore, the analysis of the change of the direction of the neutron nuclear moment in the scattering process should give us valuable additional information as compared to a determination of the change of energy and momentum direction of the neutron alone. These so-called polarization analysis experiments are discussed in a following lecture. Finally, to obtain an idea of the size of magnetic scattering relative to nuclear scattering, we can replace the matrix element in (2.71) for a spin $\frac{1}{2}$ particle by the value $I \mu_B$. This gives us an "equivalent" scattering length for magnetic scattering of 2.696 fm for a spin $\frac{1}{2}$ particle. This value corresponds quite well to the scattering length of cobalt, which means that magnetic scattering is comparable in magnitude to nuclear scattering.

In contrast to nuclear scattering, we obtain for magnetic scattering a directional term: neutrons only "see" the component of the magnetization perpendicular to the scattering vector (see Figure 2.16).

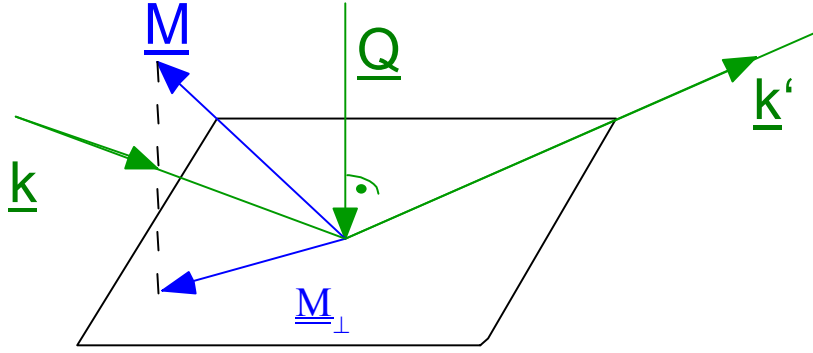


Fig. 2.16: For magnetic neutron scattering, only the component \underline{M}_\perp of the magnetization perpendicular to the scattering vector \underline{Q} is of relevance.

A second specialty of magnetic scattering as compared to nuclear scattering is the existence of the *magnetic form factor*. How the form factor comes about is most easily understood in the simple case of pure spin scattering, i. e. for atoms with spherical symmetric ($L = 0$) ground state, such as Mn^{2+} or Fe^{3+} . Moreover, the derivation is simplified for ionic crystals, where the electrons are located around an atom. We denote the spin operators of the electrons of atom i with \underline{s}_{ik} . The spatial co-ordinates of the electron number k in atom i are $\underline{r}_{ik} = \underline{R}_i + \underline{t}_{ik}$, where \underline{R}_i denotes the position vector to the nucleus of atom i . Now we proceed to separate the intra-atomic quantities. We can write the operator for the magnetization density as:

$$\underline{M}_S(\underline{r}) = -2\mu_B \sum_{ik} \delta(\underline{r} - \underline{r}_{ik}) \cdot \underline{s}_{ik} \quad (2.75)$$

The Fourier transform of this magnetization density is calculated to:

$$\underline{M}(\underline{Q}) = \int \underline{M}_S(\underline{r}) e^{i\underline{Q} \cdot \underline{r}} d^3 r = \sum_{ik} e^{i\underline{Q} \cdot \underline{r}_{ik}} \underline{s}_{ik} = \sum_i e^{i\underline{Q} \cdot \underline{R}_i} \sum_k e^{i\underline{Q} \cdot \underline{t}_{ik}} \cdot \underline{s}_{ik} \quad (2.76)$$

To calculate the scattering cross section, we now have to determine the expectation value of this operator for the quantum mechanical state of the sample averaged over the thermodynamic ensemble. This leads to

$$\underline{M}(\underline{Q}) = -2\mu_B \cdot f_m(\underline{Q}) \cdot \sum_i e^{i\underline{Q} \cdot \underline{R}_i} \cdot \underline{S}_i \quad (2.77)$$

The single differential cross section for elastic scattering is thus given by:

$$\frac{d\sigma}{d\Omega} = (\gamma_n r_0)^2 \left| f_m(\underline{Q}) \sum_i \underline{S}_{i\perp} e^{i\underline{Q} \cdot \underline{R}_i} \right|^2 \quad (2.78)$$

Here, $f_m(\underline{Q})$ denotes the form factor, which is connected with the spin density of the atom via a Fourier transform:

$$f_m(\underline{Q}) = \int_{Atom} \rho_s(\underline{r}) e^{i\underline{Q} \cdot \underline{r}} d^3 r \quad (2.79)$$

With the form (2.78), we have expressed the cross section in simple atomic quantities, such as the expectation values of the spin moment \underline{S}_i at the various atoms. The distribution of the spin density within an atom is reflected in the magnetic form factor (2.79).

For ions with spin and orbital angular momentum, the cross section takes a significantly more complicated form [4]. Under the assumption that spin- and orbital- angular momentum of each atom couple to the total angular momentum \underline{J}_i (L/S -coupling) and for rather small momentum transfers (the reciprocal magnitude of the scattering vector has to be small compared to the size of the electron orbits), we can give a simple expression for this cross section in the so-called *dipole approximation*:

$$\frac{d\sigma}{d\Omega} = (\gamma_n r_o)^2 \cdot \left| \frac{g_J}{2} f_m(Q) \sum_i J_{i\perp} e^{iQ \cdot R_i} \right|^2 \quad (2.80)$$

Here the magnetic form factor writes:

$$f_m(Q) = \langle j_0(Q) \rangle + C_2 \langle j_2(Q) \rangle \quad (2.81)$$

g_J denotes the Lande g-factor, $C_2 = \frac{2}{g_J} - 1$ and

$$\langle j_l(Q) \rangle = 4\pi \int_0^\infty j_l(Qr) R^2(r) r^2 dr \quad (2.82)$$

are the spherical transforms of the radial density distributions $R(r)$ with the spherical Bessel functions $j_l(Qr)$. For isolated atoms, the radial part $R(r)$ has been determined by Hartree-Fock-calculations and the functions $\langle j_0(Q) \rangle$ and $\langle j_2(Q) \rangle$ in (2.82) have been tabulated [9].

Since the distribution of the magnetic field for spin and orbital angular momentum is completely different, different Q-dependencies of the corresponding form factors result. Moreover, because only the outer electrons in open shells contribute to magnetic scattering, the magnetic form factor also differs from the x-ray form factor, which is the Fourier transform of the entire electron density distribution within an atom, see Figure 2.17.

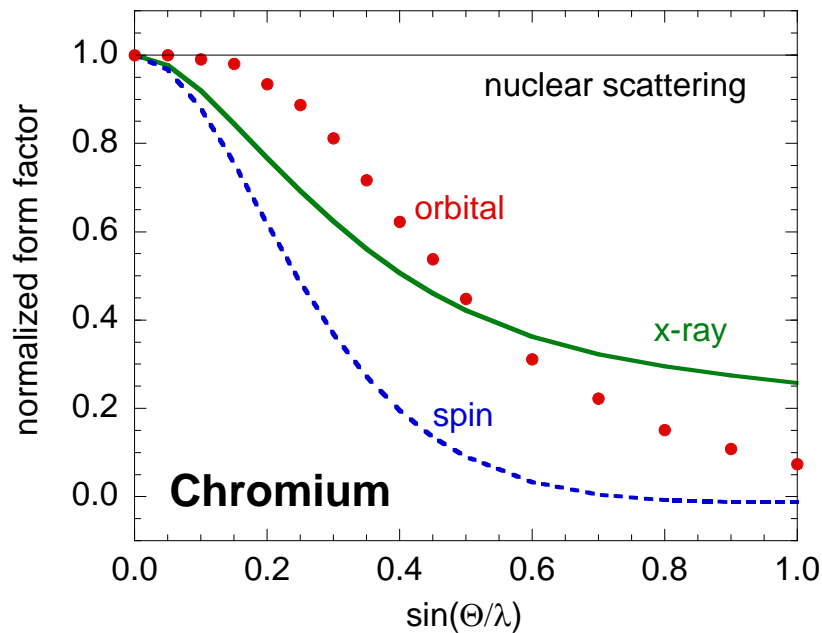


Fig. 2.17: Form-factor of Cr [10, 11]. Due to the different distribution of the magnetic field for spin S and orbital angular momentum L , a more rapid decrease of the scattering amplitude as a function of momentum transfer results for the spin form factor. For the x-ray form factor, the inner electrons play an important role, too. Therefore, the x-ray form factor drops slower as compared to the magnetic form factor. On the Å length scale of the thermal neutron wavelength, the nucleus is point-like. Therefore, nuclear scattering is independent of the momentum transfer. Finally, we want to mention that the magnetic form factor can in general be anisotropic, if the magnetization density distribution is anisotropic.

2.14 Comparison of probes

In this lecture, we have so far introduced the elementary formalism to describe the scattering process and discussed the interaction of neutrons with matter. We now want to ask the questions, for which problems in condensed matter research, neutrons can be utilized successfully also in comparison to other probes, such as x-ray scattering or electron microscopy and electron scattering. To answer these questions, we have to look at the ranges of energies, wavelength or scattering vector, which can be covered by various probes as well as the different contrast mechanisms.

Figure 2.18 shows a double logarithmic plot of the dispersion relation "wavelength versus energy" for the three probes neutrons, electrons and photons. The plot demonstrates, how thermal neutrons of energy 25 meV are ideally suited to determine interatomic distances in the order of 0.1 nm, while the energy of x-rays or electrons for this wavelength is much higher. However with modern techniques at a synchrotron radiation source, energy resolutions in the meV-region become accessible even for photons of around 10 keV corresponding to a relative energy resolution $\Delta E/E \approx 10^{-7}$! The graph also shows that colloids with a typical size of 100 nm are well suited for the investigation with light of energy around 2 eV. These length scales can, however, also be reached with thermal neutron scattering in the small angle region. While Figure 18 thus demonstrates for which energy-wave-length combination a certain probe is particularly useful, modern experimental techniques extend the range of application by several orders of magnitude.

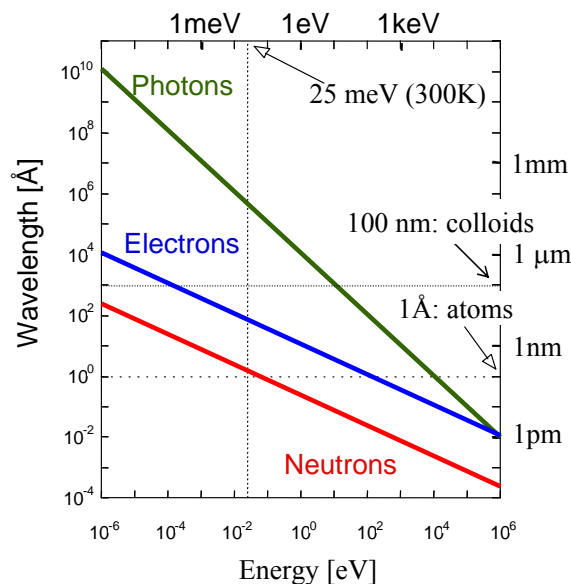


Fig. 2.18: Comparison of the three probes - neutrons, electrons and photons - in a double logarithmic energy-wavelength diagram.

It is therefore useful to compare the scattering cross sections as it is done in Figure 2.19 for x-rays and neutrons. Note that the x-ray scattering cross sections are in general a factor of 10 larger as compared to the neutron scattering cross sections. This means that the signal for x-ray scattering is stronger for the same incident flux and sample size. But caution has to be applied that the conditions for kinematical scattering are fulfilled. For x-rays, the cross section depends on the number of electrons and thus varies in a monotonic fashion throughout the periodic table. Clearly it will be difficult to determine hydrogen positions with x-rays in the presence of heavy elements such as metal ions. Moreover, there is a very weak contrast between neighboring elements as can be seen from the transition metals Mn, Fe and Ni in Figure

2.19. However, this contrast can be enhanced by anomalous scattering, if the photon energy is tuned close to the absorption edge of an element. Moreover, anomalous scattering is sensitive to the anisotropy of the local environment of an atom. For neutrons the cross section depends on the details of the nuclear structure and thus varies in a non-systematic fashion throughout the periodic table. As an example, there is a very high contrast between Mn and Fe. With neutrons, the hydrogen atom is clearly visible even in the presence of such heavy elements as Uranium. Moreover there is a strong contrast between the two Hydrogen isotopes H and D. This fact can be exploited for soft condensed matter investigations by selective deuteration of certain molecules or functional groups. This will vary the contrast within the sample.

Finally, both neutrons and x-rays allow the investigation of magnetism on an atomic scale. Magnetic neutron scattering is comparable in strength to nuclear scattering, while non-resonant magnetic x-ray scattering is smaller than charge scattering by several orders of magnitude⁶. Despite the small cross sections, non-resonant magnetic x-ray Bragg scattering from good quality single crystals yields good intensities with the brilliant beams at modern synchrotron radiation sources. While neutrons are scattered from the magnetic induction within the sample, x-rays are scattered differently from spin and orbital momentum and thus allow one to measure both form factors separately. Inelastic magnetic scattering e.g. from magnons or so called quasielastic magnetic scattering from fluctuations in disordered magnetic systems is a clear domain of neutron scattering and cannot be done with x-rays up to now. Finally, resonance exchange scattering XRES allows one not only to get enhanced intensities, but also to study magnetism with element- and band sensitivity [12].

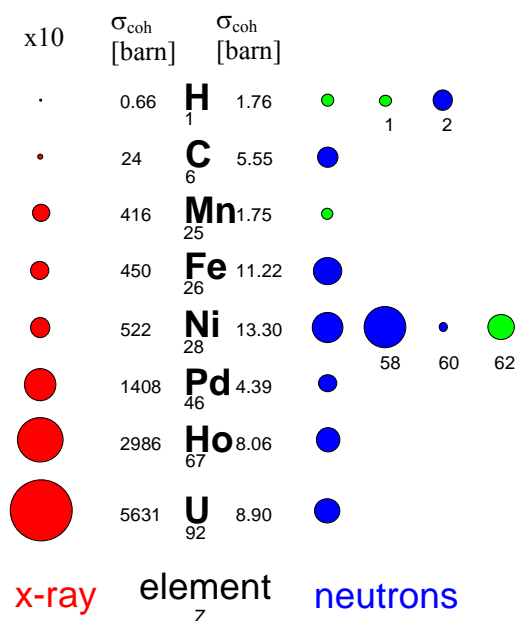


Fig. 2.19: Comparison of the coherent scattering cross-sections for x-rays and neutrons for a selection of elements. The area of the colored circles represent the scattering cross section, where in the case of x-rays a scale factor 10 has to be applied. For neutrons, the blue and green circles distinguish the cases where the scattering occurs with or without a phase shift of π . For ^1_1H and $^{28}_{28}\text{Ni}$, scattering cross sections for certain isotopes are given in addition to the averaged values for the natural abundancies.

⁶ Typically between 6 to 9 orders of magnitude.

With appropriate scattering methods, employing neutrons, x-rays or light, processes in condensed matter on very different time and space scales can be investigated. Which scattering method is appropriate for which region within the "scattering vector Q - energy E plane" is plotted schematically in Figure 2.20. A scattering vector Q corresponds to a certain length scale, an energy to a certain frequency, so that the characteristic lengths and times scales for the various methods can be directly determined from the Figure. Examples for applications and information on instrumentation will follow in subsequent lectures.

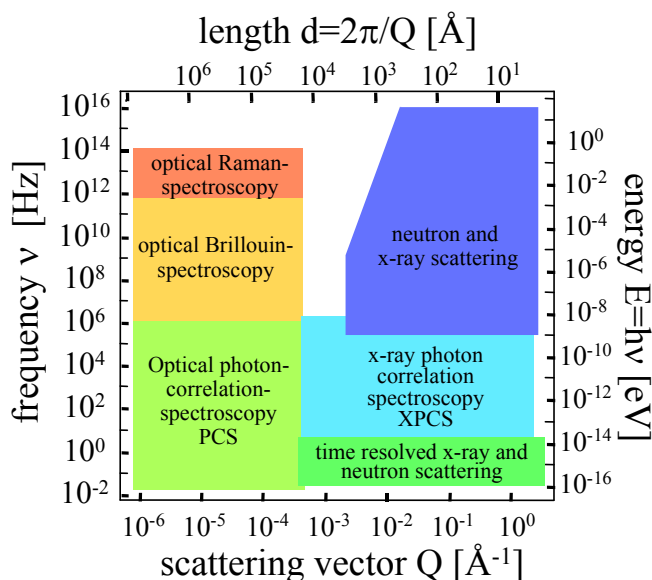


Fig. 2.20: Regions in frequency ν and scattering vector Q or energy E and length d , which can be covered by various scattering methods.

References

- [1] G. L. Squires "Introduction to the Theory of Thermal Neutron Scattering" Dover 1997
- [2] K. Sköld, D. Price (Eds.) "Methods of Experimental Physics" Neutron Scattering Part A-C Academic Press 1987
- [3] J. M. Cowley "Diffraction Physics" North Holland, Amsterdam 1995
- [4] S. W. Lovesey "Theory of neutron scattering from condensed matter" Clarendon Press, Oxford, 1987
- [5] A. Furrer, J. Mesot, T. Strässle "Neutron Scattering in Condensed Matter Physics" World Scientific, London, 2009
- [6] B. W. Batterman, H. Cole "Dynamical Diffraction of X-Rays by Perfect Crystals" Rev. Mod. Phys. **36** (1964), 681 - 717.
- [7] A. Dianoux, G. Lander (Eds.) "Neutron Data Booklet", Institute Laue-Langevin (2002) - see also [8] -
- [8] D. E. Garber, R. R. Kinsey "Neutron Cross-Section II" BNL-Report (1976), also: S. Mughabghab "Atlas of Neutron Resonances" Elsevier (2006)
- [9] E. Price (Ed.) "International Tables for Crystallography, Volume C" International Union of Crystallography (2004) - see also [6] -
- [10] J. Stempfer et al. Eur. Phys. J B **14** (2000), 63 - 72
- [11] J. Stempfer et al. Physica B **267 - 268** (1999), 56 - 59
- [12] Th. Brückel "Scattering Techniques II: Magnetic X-Ray Scattering" Schriften des Forschungszentrum Jülich, Materie und Material **26** (2006), B5.1 - B5.34

